sustainability

MDPI

Article

Novel Ultra-High-Performance Concrete (UHPC) Enhanced by Superhydrophobic and Self-Luminescent Features

Ahmad Rizwan Mumtaz [1], Natalija Bede Odorčić [2], Núria Garro [3], Samo Lubej [1], Andrej Ivanič [1], Antonio Comite [4], Marcello Pagliero [4] and Gregor Kravanja [1,5,*]

[1] Faculty of Civil Engineering, Transportation and Architecture, University of Maribor, Smetanova 17, 2000 Maribor, Slovenia; ahmadrizwan.mumtaz@student.um.si (A.R.M.); samo.lubej@um.si (S.L.); andrej.ivanic@um.si (A.I.)
[2] Faculty of Civil Engineering, University of Rijeka, 51000 Rijeka, Croatia; natalija.bede@uniri.hr
[3] Institute of Materials Science, Universidad de Valencia, 46980 Valencia, Spain; nuria.garro@uv.es
[4] Department of Chemistry and Industrial Chemistry, University of Genoa, Via Dodecaneso 31, 16146 Genoa, Italy; antonio.comite@unige.it (A.C.); marcello.pagliero@unige.it (M.P.)
[5] Faculty of Chemistry and Chemical Engineering, University of Maribor, Smetanova 17, 2000 Maribor, Slovenia
* Correspondence: gregor.kravanja@um.si

Abstract: This study explores the potential of using basalt reinforced UHPC by incorporating simultaneously self-cleaning and self-luminescent features, paving the way for sustainable advancements in civil engineering. New green formulations of UHPC were developed by integrating supplementary cementitious materials and optimizing water to the binder ratio, followed by using basalt fibers to enhance strength and ductility. The fabricated samples with high particle-packing density exhibit sufficient workability and compressive strength up to 136 MPa, and, when incorporating basalt fibers, a notable reduction in brittleness. The inner microstructure of basalt fibers was observed to be smooth, homogeneously distributed, and well adhered to the UHPC matrix. To ensure the desired long-lasting visual appearance of decorative UHPC and reduce future maintenance costs, a time-effective strategy for creating a light-emitting biomimetic surface design was introduced. The samples exhibit high surface roughness, characterized by micro to nano-scale voids, displaying superhydrophobicity with contact angles reaching up to 155.45°. This is accompanied by roll-off angles decreasing to 7.1°, highlighting their self-cleaning features. The self-luminescence feature showcased intense initial light emission, offering a potential energy-efficient nighttime lighting solution.

Keywords: UHPC; basalt fibers; mechanical properties; morphology; superhydrophobic; self-luminescence

Citation: Mumtaz, A.R.; Bede Odorčić, N.; Garro, N.; Lubej, S.; Ivanič, A.; Comite, A.; Pagliero, M.; Kravanja, G. Novel Ultra-High-Performance Concrete (UHPC) Enhanced by Superhydrophobic and Self-Luminescent Features. *Sustainability* **2024**, *16*, 1068. https://doi.org/10.3390/su16031068

Academic Editor: Junsheng Su

Received: 28 December 2023
Revised: 18 January 2024
Accepted: 22 January 2024
Published: 26 January 2024

1. Introduction

Ultra-High-Performance Concrete (UHPC) has become a prominent player in the domain of sustainable construction materials, attracting substantial interest due to its outstanding mechanical properties and enduring durability [1]. The characteristics of UHPC, including strength, ductility, durability, and flexibility in aesthetic design, make it an exceptionally advanced and versatile material [2]. The resilience of UHPC is evaluated based on its resistance to water and chloride-ion permeability, carbonation, freeze–thaw cycles, resistance to chemical attacks, and susceptibility to the alkali–silica reaction, abrasion, and fire [3]. Therefore, UHPC has the potential to become the preferred material for concrete structures in various applications and environments. The addition of fibers to concrete has proven to be an effective measure to increase the durability of concrete structures subjected to different loading conditions such as impacts or fatigue loads. For example, Gu et al. [4] showed that the flexural fatigue life of high-strength steel fiber-reinforced concrete is more than 106% higher than that without fibers. Although UHPC is renowned for its remarkable durability and typically reinforced with steel fibers, a potential concern

arises. These steel fibers are susceptible to corrosion from chloride ions, which can impact the overall performance of UHPC. For instance, the erosion of steel fibers within UHPC could lead to an increase in the porosity of the interface transition zone (ITZ) between the steel fiber and concrete matrix [5]. To address this vulnerability, a promising alternative comes in the form of basalt fibers, offering a novel and corrosion-resistant reinforcement solution [6]. The use of fibers with different volume contents has the potential to improve the mechanical properties of concrete when the fibers are uniformly distributed in the matrix [7]. However, achieving a uniform distribution of fibers is challenging, especially at higher fiber contents. Fibers tend to agglomerate in the cement matrix, leading to an increase in the number of pores of different sizes and, consequently, a deterioration in the mechanical properties. Therefore, to thoroughly investigate the mechanical properties of fiber-reinforced cement composites, it is essential to explore the relationship between the microscopic and macroscopic properties of these materials. Various methods, such as scanning electron microscopy (SEM), transmission electron microscopy (TEM), or X-ray micro-computed tomography (micro-CT), have been employed to assess the microstructure of concrete composites. Among these methods, X-ray micro-CT holds a distinct advantage due to its non-destructive nature. Thomoglou et al. [8] used this method to determine the correlation between the mechanical properties of nano-reinforced cement mortar with density and porosity. It was found that there is a linear correlation between density and pore size distribution with mechanical properties, emphasizing that compressive strength correlates more strongly than flexural strength.

While UHPC boasts superior mechanical properties and outstanding durability, it falls short of meeting engineering performance criteria and tends to be considerably more expensive than conventional concrete mixtures [9]. This cost disparity is primarily due to the high cement consumption in UHPC production, typically reaching up to 1100 kg/m^3 [2]. Thus, the current trend is towards producing UHPC with low energy consumption and a reduced carbon footprint by incorporating supplementary cementitious materials (SCMs) [10]. Among various SCMs such as fly ash (FA), slag cement (SC), and microsilica (MS), metakaolin (MK) stands out as a material with significant potential for contributing to a sustainable future [11]. Enhancing the early strength of UHPC requires the development of novel and efficient accelerators. The scientific exploration of nanomaterial enhancements in this field is still insufficiently examined. Nanomaterials, such as nano-TiO_2, carbon nanotubes, nano-SiO_2, nano-$CaCO_3$, and nano-alumina, assume a pivotal role as modifiers in cement paste [12]. For example, incorporating nano-SiO_2 at a dosage of 1 wt.% resulted in an approximately 20% increase in the 1-day compressive strength of UHPC [13].

Common applications of UHPC include the construction of bridges, wind turbine towers, marine structures, precast elements, military construction, and tunnels. It is also utilized in the creation of decorative facade panels for buildings, offering both aesthetic appeal and structural integrity. UHPC's unique properties allow for intricate and innovative architectural designs, making it an ideal choice for the development of unique and aesthetically pleasing structures [14]. The issues emerge over time, as the diffusion and deposition of pollutants on the surface of UHPC could significantly affect the appearance and escalate the financial and material resources required for its maintenance. UHPC is prone to the easy accumulation of pollutants, leading to a diminished gloss and an increase in stains. Currently, there is a lack of research exploring the self-cleaning performance of decorative UHPC on both domestic and international fronts. Nevertheless, a substantial body of research is dedicated to the self-cleaning aspects of concrete, with a primary focus on surface-coating methods [15–19]. Super water-repellent surfaces can be achieved by creating micro/nano robustness surface designs. Nanoparticles play a crucial role in nanocoatings, as they can readily form nanostructures on their surfaces. Considering UHPC composition, utilizing cement is beneficial as it has a good interface bonding with inorganic nanoparticles, which are the key factors that enhance its surface strength [20]. Commonly used inorganic nanoparticles, such as nano-SiO_2, nano-A_2O_3, and nano-TiO_2, can facilitate

cross-linking or covalent bonding among substrates and coatings, thereby enhancing the durability and protecting concrete [21].

Achieving a self-cleaning surface, biomimetic superhydrophobic surface design is crucial [22]. Superhydrophobic surface involves applying nano-improved hydrophobic substances either on the concrete surface or within shallow surface pores. This process creates continuous protective coatings, enhancing long-term durability upon solidification [23]. Enhanced by superhydrophobicity, concrete has the capacity to further improve its characteristics, achieving multiple functionalities that align with sustainability principles.

The incorporation of self-luminescent properties into concrete materials represents an innovative concept within the realm of civil engineering, and has recently become a focal point of research attention [24]. Incorporating self-illumination properties into concrete structural components by integrating built-in illumination devices or luminescent materials presents a potential solution. This approach not only has the capacity to conserve energy and minimize ecological light pollution, but also to address challenges associated with the uneven illumination and glare often induced by conventional streetlamps [25]. Advanced economies, including Germany, the United States, and France, have initiated research and development endeavors in the realm of self-illuminating concretes [26]. About 30% of global power production is dedicated to end-use in civil sectors, and almost 60% of the world's electric power is utilized by commercial and residential buildings [27]. From the perspective of minimizing energy consumption, creating self-luminescent material is a necessity.

The objective was to enhance the functionality and long-lasting visual appearance of basalt-reinforced UHPC. Simultaneously, the goal was to decrease the energy consumption associated with the night lighting of UHPC infrastructure. To align with advanced sustainability practices in civil engineering, the surface of UHPC was modified for the first time to achieve simultaneously self-cleaning and self-luminescent properties.

Envisioning the smart cities of tomorrow, this novel UHPC might play a central role in shaping intelligent infrastructure. In the realm of high-rise buildings, the novel UHPC offers an opportunity to redefine construction standards. Facades and structural components benefit from enhanced strength and durability, ensuring that skyscrapers withstand the test of time and environmental challenges. The superhydrophobic feature adds an extra layer of protection, preserving the aesthetic appeal of the building for years to come. The self-luminescent feature provides a passive lighting solution that contributes to safety and a futuristic luminescence appearance in the dark without relying on external power sources. Furthermore, bridge decks illuminated by a soft, self-generated glow can be constructed with superior resistance to water absorption. This not only extends the lifespan and safety of the structure but also results in substantial cost savings. In the energy sector, this UHPC can reinforce the foundations of wind turbines and support structures for solar panels, ensuring their longevity and visibility through renewable energy installations.

In the first part, this article explores a cutting-edge advancement in UHPC by introducing a novel mix design that incorporates SCMs such as metakaolin (MK) and microsilica (MS), along with basalt fibers serving as an alternative for concrete reinforcement. This innovative UHPC formulation was aimed at enhancing both strength and sustainability. The optimization of the w/b ratio corresponds to compression strength and rheo-logical properties. The influence of SCMs and basalt fibers on the mechanical properties of UHPC was studied in detail. In the second part of this article, attention is directed towards the integration of superhydrophobicity and luminescence integration into UHPC. A double-layer coating was introduced to achieve a self-cleaning surface with a low water roll of angles and durable self-luminescence. The detailed analysis covers wettability, surface morphology, and the roughness of the UHPC. Additionally, it includes the measurements of light emittance in the dark, providing insights into the mechanisms supporting these advanced features.

2. Materials and Methods

2.1. Raw Materials

White cement 52.5 R (CEM 1), commercially known as Salonit Ultrasal 52.5 R, with a specific gravity of 3.1, was pursued by Salonit Anhovo d.o.o, Deskle, Slovenia. Micro silica (MS) with a specific gravity of 2.2 and metakaolin (MK) with a specific gravity of 2.1 were used as supplementary cement materials (SCMs). Fine aggregates and fillers consisting of sand with a fineness modulus of 2.81 and limestone powder (LP) with a specific gravity of 2.6, respectively were sourced. A locally available mineral additive MS and fine aggregates and fillers were provided by Murexin d.o.o., Buzin, Slovenia. MK, commercially known as MELAPRET AAS 100, with a density of 890 kg/m^3, was sourced from Melanin d.o.o, Kočevje, Slovenia. The water used in the mixture was tap water, and it was accompanied by a third-generation polycarboxylate superplasticizer (SP). As concrete reinforcement, 12 mm long basalt fibers were used with a specific gravity of 2.6. The hydrophobic compound poly(methyl)hydrogen siloxane (PMHS) with a specific of gravity 1.1 and silicon dioxide (SiO_2) nano-powder with a 10–20 nm particle size (BET) and 99.5% trace metals basis were purchased from Sigma Aldrich (St. Louis, MO, USA). Low-cost polyester-based covering meshes with the sizes of the inner squares being 200 µm were kindly donated by Konus Konex d.o.o, Slovenske Konjice, Slovenia. The luminescent powder (lum) used in the preparation of the luminescent coating is strontium aluminate luminescence powder, which has a specific gravity of 3.73 and was supplied by Samson Kamnik d.o.o, Kamnik, Slovenia. All materials were used with 0% moisture contents. The Laser Particle Sizer ANALYSETTE 22 (Fritsch NanotTech, Helmbrechts, Germany) was used to measure the particle sizes and cumulative distribution of powder raw materials (Figure 1). UHPC mixtures are commonly formulated using fine aggregate [28].

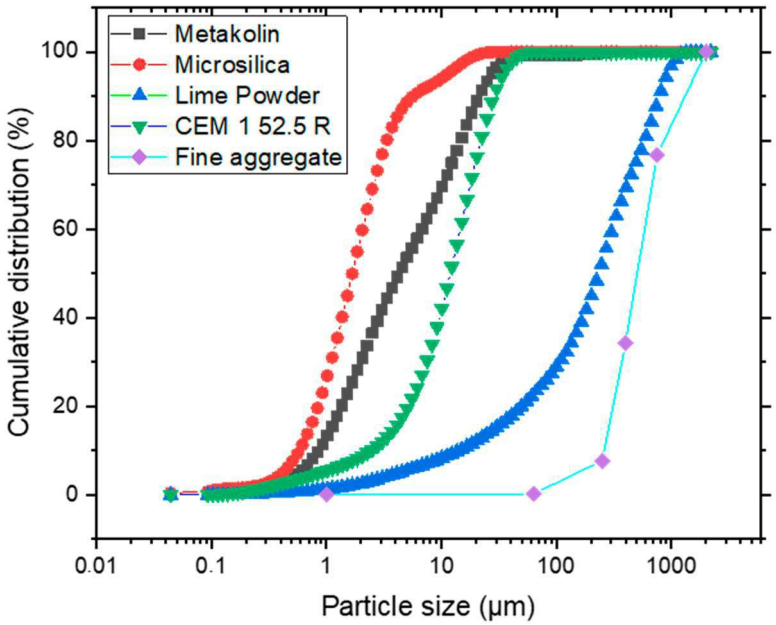

Figure 1. Particle size distribution for: metakaolin (MK), lime powder (LP), micro silica (MS), cement (CEM 1 52.5 R) and fine aggregate.

The chemical composition of UHPC compounds was determined using an X-ray fluorescence (XRF) analyzer NITON Thermo Fisher Scientific, Waltham, MA, USA, and is provided in Table 1.

Table 1. Chemical composition of UHPC compounds, as characterized by X-ray fluorescence (XRF).

Chemical Composition (wt.%)									
Oxide	**CaO**	**SiO_2**	**Al_2O_3**	**Fe_2O_3**	**SO_3**	**MgO**	**Na_2O**	**K_2O**	**TO_2**
CEM 52.5 R	64.80	22.20	5.40	3.30	3.20	0.50	0.20	0.20	0.20
MK	0.20	54.00	42.00	0.90	0.50	0.20	0.70	0.10	0.50
MS	0.70	95.00	2.30	0.50	0.10	0.10	0.10	0.10	0.10
LP	83.20	6.40	1.50	1.00	0.20	1.20	0.00	0.00	0.00

2.2. Mix Design

To produce this novel UHPC enhanced by superhydrophobic and self-luminescent features, full compliance with ASTM C1856/C1856M-17 was ensured [29]. Initially, reference concrete (REF) was manufactured using normal sand, cement 52.5 R, and tape water with an aggregate-to-cement (a/c) ratio of 3 and with a water-to-cement (w/c) ratio of 0.5.

A series of experiments were then conducted to fabricate this innovative, sustainable, and environmentally friendly UHPC. Initially, MS ranging from 0.5% to 1.5% and UHPC with MK from 0.5% to 1.5%, without basalt fibers (BF), were individually used as cement replacements to determine the optimal mixture. The fixed quantities include LP, fine sand, and 3% superplasticizer. The mixture with a 10% cement replacement of both MS and MK is identified as the optimal blend. Subsequently, this mixture with 10% MS and MK is further tested with the introduction of BF ranging from 0.25% to 1.5% by volume of the binder. The mixture with 1% of BF was selected for the subsequent fabrication of a superhydrophobic and self-luminescent UHPC, incorporating both MS and MK separately.

The water-to-binder ratio (w/b) was optimized during experimental work, initially set at w/b 0.22, and a slump test was conducted as per to SIST-EN-1015-3 [30]. Table 2 presents the composition of superhydrophobic and self-luminescent UHPC. Three cubical samples of each mix were cast with dimensions of 70 mm × 70 mm × 70 mm for compression tests in compliance with ASTM C109/C109M-99 [31], and three rectangular samples of 40 mm × 40 mm × 160 mm for each mix were cast for flexural strength testing in accordance with HRN EN 196-1 [32] (Figure 2).

Table 2. Composition of superhydrophobic and self-luminescent UHPC.

Material	**UHPC MS**	**UHPC MK**	**UHPC MS 0.5%**	**UHPC MS 1%**	**UHPC MS 1.5%**	**UHPC MK 0.5%**	**UHPC MK 1%**	**UHPC MK 1.5%**
Weight (Kg)								
CEM 52.5	746.00	746.00	746.00	746.00	746.00	746.00	746.00	746.00
Fine Sand	954.00	954.00	954.00	954.00	954.00	954.00	954.00	954.00
MK	0.00	74.60	0.00	0.00	0.00	74.60	74.60	74.60
MS	74.60	0.00	74.60	74.60	74.60	0.00	0.00	0.00
Binder	820.60	820.60	820.60	820.60	820.60	820.60	820.60	820.60
LP	199.00	199.00	199.00	199.00	199.00	199.00	199.00	199.00
Water *	197.76	197.76	197.76	197.76	197.76	197.76	197.76	197.76
SP %	31.18	31.18	31.18	31.18	31.18	31.18	31.18	31.18
Fiber %	0.00	0.00	13.00	26.00	39.00	13.00	26.00	39.00

* Water was varied, from 0.22 up to 0.28 w/b.

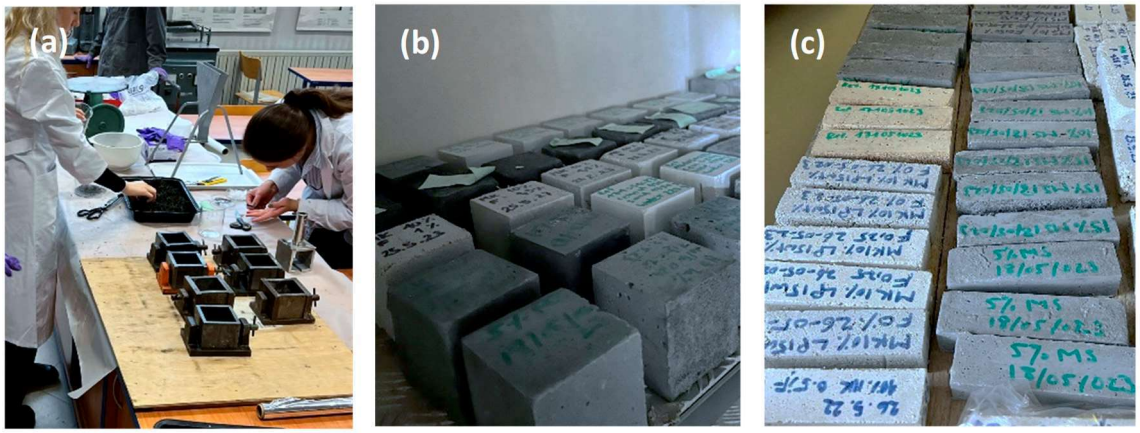

Figure 2. For each mixture, (**a**) cubical samples (70 mm × 70 mm × 70 mm) and rectangular samples (40 mm × 40 mm × 160 mm) were prepared, and (**b**,**c**) samples were cured under 98% relative humidity and 298 K for 28 days.

Advanced Light-Emitting Biomimetic Surface Design

A new cost- and time-effective fabrication strategy for the advanced light-emitting biomimetic surface designing of UHPC is introduced (Figure 3).

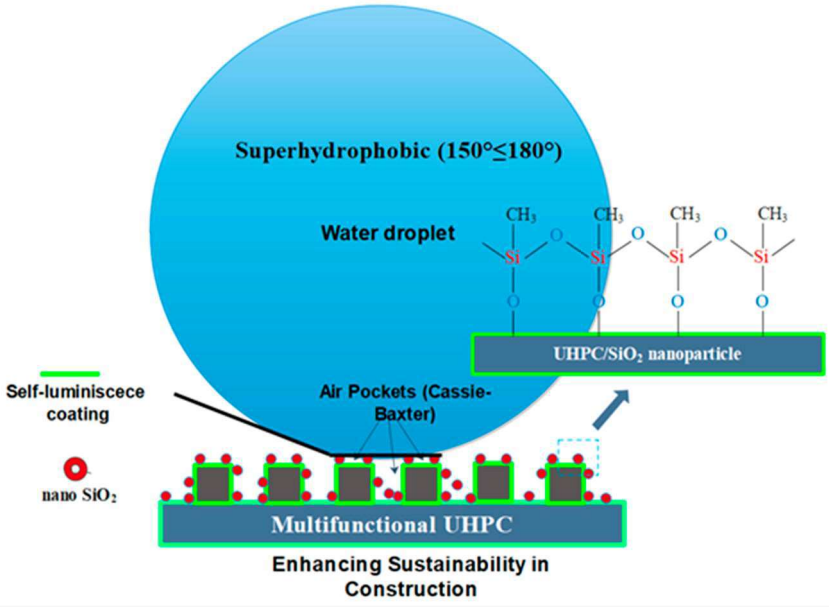

Figure 3. Schematic presentation of UHPC integrating with self-luminescence and superhydrophobicity.

Before pouring the concrete, the inner sidewalls of the molds were coated with a polyester mesh of square cross-section with sides of 200 µm to obtain the desired micro robustness. UHPC is characterized by dense particle packing and a low water–cement ratio, as outlined in Section 3.1. Consequently, to achieve water repellency, there is no need for internal hydrophobic additives in the concrete mix [33]. After the curing of the concrete into a rigid mass (for approximately 1 day), the meshes were removed, and the samples underwent additional curing for 28 days according to standards SIST EN 12390-1 [34] and SIST EN 12390-2 [35]. To enhance micro robustness and achieve self-luminescence, a transparent coating made of concrete varnish and submicron luminescent powder with greenish-yellow afterglow was applied to the surface. To achieve surface nano-robustness, a nanoparticle-based suspension was prepared using a simple and scalable method outlined in our previous work [22]. SiO_2 nanoparticles (0.6 g) were dispersed in ethanol (100 mL) for 20 min under ultrasonication, and then treated for 10 min with a high-speed homogenizer

at 10,000 rpm. Subsequently, polymethylhydrosiloxane (PMHS) (25 mL) was added slowly, drop by drop, under magnetic stirring for over 30 min. A suspension based on ivory white SiO_2 nanoparticles was sprayed from left to right at a speed of 5 cm/s, maintaining a nozzle distance of at least 10 cm from the surface. After completing the spraying process, the samples were cured at room temperature for a few days. The surface of UHPC resulted in a dual-level fractal structure by submillimeter structure and nano-level roughness to ensure water repellent surfaces with Cassie-Baxter states and self-luminescence.

2.3. Characterization Methods

2.3.1. The Wet Particle-Packing Method

The properties of the composite material being formed are certainly managed by the particle-packing behavior of granular materials [36]. UHPC, widely acknowledged as a practical and prominent concrete material, not only boasts ultra-high strength but also demonstrates outstanding performance in both fresh and hardened states [37]. The ongoing chase for an extremely low water-to-cement ratio aims to achieve a higher strength, which can be enhanced by using supplementary cementitious materials (SCMs) [38]. This practice is intended not only to enhance sustainability but also to improve the packing density of the binder system [39]. The wet particle-packing method is adopted for the design of a state-of-the-art green UHPC recipe.

The water-to-solid (w/s) ratio by volume, represented as the wet particle density (WPD) $\varnothing$, is defined as the maximum solid concentration calculated by Equation (1). The solid volume in the mold, denoted as V_c, is computed by Equation (2):

$$\varnothing = \varnothing_{max} = V_c / V \tag{1}$$

$$V_c = \frac{M}{\rho_w \mu_w + \rho_\alpha R_\alpha + \rho_\beta R_\beta + \rho_\gamma R_\gamma} \tag{2}$$

In Equation (3), M and V refer to the mass and volume of the mixture in the mold, ρ_w to the density of water, ρ_α, ρ_β, and ρ_γ to the solid density of different binder materials, and R_α, R_β, and R_γ to the volumetric ratios of binder materials. Then, minimum void ratio (u) is calculated by Equation (3):

$$u = (V - V_c)/V_c \tag{3}$$

The following steps are performed to exercise the wet particle-packing method:

1. Develop a series of mix designs using the same binder system but with varying water-to-solid (w/s) ratios, starting from 1.0 and gradually decreasing this value;
2. Combine half of the cementitious materials, half of the SP, and all the required water in a mixing bowl. Mix for 3 min, preferably pre-mixing the dry powder;
3. Divide the remaining cementitious materials and SP into four equal portions. Mix for 2 min before adding each portion successively;
4. Pour the mixture into a cylinder mold;
5. Repeat steps (1) to (4) for each subsequent mix, gradually reducing the w/s ratio until reaching the point where the maximum solid concentration is identified.

2.3.2. Slump Test

In the mini-slump test that was carried out according to SIST-EN-1015-3 [30], a smooth plate was utilized, upon which a truncated conic mold was positioned, filled with UHPC, and subsequently lifted upward. The spread diameter of the mortar was then measured in two perpendicular directions, and the average of these diameters was recorded as the slump flow deformation of the concrete.

2.3.3. Compression and Flexural Strength Tests

The compressive and flexural strength tests for each concrete mixture were carried out in accordance with the HRN EN 196-1 test standard [32]. Since the fibers have a relatively small influence on the compressive strength of concrete, the same tests are applicable for samples with and without fibers. A universal testing machine with a maximum load capacity of 600 kN was used for the compression tests. In this method, the compressive strength is determined on the halves of the prismatic specimens previously tested in bending, with the load transferred through steel plates measuring 40 mm × 40 mm, which corresponded to the loading area of the prism. Six (6) specimens were tested for each concrete mix.

The mechanical test of primary interest for composites with fibers is the flexural (bending) test, as the addition of fibers typically results in significant improvements in properties such as toughness and crack control propagation. The flexural behavior of the test specimens was determined following the HRN EN 196-1 test standard [32], with some modifications in the loading arrangement. However, the testing conditions were consistent for all concrete mixtures.

Prismatic test specimens measuring 40 mm × 40 mm × 160 mm underwent a three-point bending test, concentrating the force in the middle of a 100 mm span, as illustrated in Figure 4. The tests employed constant rate displacement control. Throughout testing, the load–displacement history was recorded until a fracture occurred to capture post-peak behavior. To record midspan vertical displacement, 2D digital image correlation (DIC) method and linear variable differential transformer (LVDT) sensors were used simultaneously. Each concrete mixture underwent testing using three (3) specimens. Flexural tests were conducted using a universal testing machine with a maximum capacity of 50 kN.

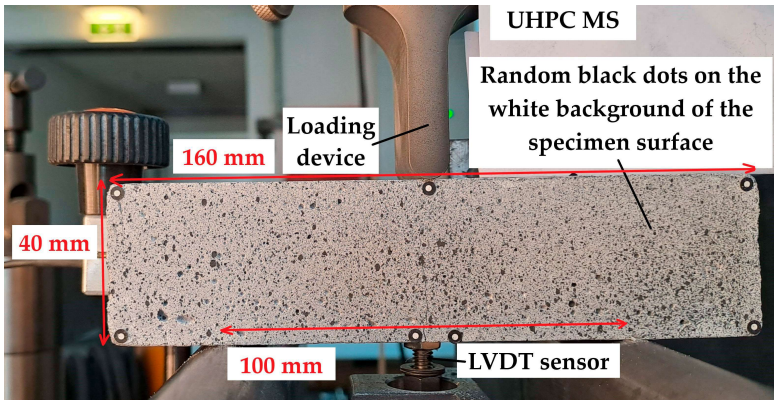

Figure 4. The test arrangement using beam with third-point loading.

2.3.4. Microstructure Observation

The microstructure of cement composite samples was studied by means of electron microscopy. The surface and internal structures were observed using an FE-SEM (Supra 40 VP, Carl Zeiss, Oberkochen, Germany) coupled with energy-dispersive X-ray spectrometry (EDS) and back-scattering (BS). The FE-SEM/EDS/BS observation and analysis of the basalt fibers in the inner cross-section of the samples was fractured and mechanically flat-polished using a series of polishing steps with abrasives with progressively finer grain sizes. The observation of the surface morphology was carried out on smaller specimens carefully fractured from the main cementitious samples by keeping part of the surface area of interest intact. All the specimens were fixed on a microscopy stub by using a carbon-based adhesive tape and sputter-coated with a thin film of carbon as of conductive material to prevent the build-up of electric charge during electron scanning by means of a high vacuum evaporator (Polaron 6700, Quorum Technologies, Laughton, UK). To provide the roughness of the concrete surfaces, topographic profiles were measured with a modified optical profilometer (Mahr Pocket Surf IV Portable Surface Roughness Gage, Göttingen, Germany).

2.3.5. Wettability Tests

Contact Angles (CA) and Roll-off Angles (RA) of the treated samples were measured at 293 K using a Contact Angle goniometer based on the sessile drop method. Droplets of milli-Q water (with a specific resistance of 18.2 μΩ) were formed on a concrete surface with exact sizes of 10 μL using a micropipette. A Basler acA 300-200 um digital camera equipped with a Basler Premium Lens with C-mount was connected to a computer, and the OpenDrop algorithm was used for Contact Angle calculation [40]. Detailed descriptions can be found in the literature [22].

2.3.6. Spectroscopy and Light-Emission Test

The spectral characteristics and luminous emission intensity of samples coated with luminescence powder were analyzed using a long-pass filtered Acton SP-300i from Princeton Instruments (Acton, MA, USA).

3. Results and Discussion

3.1. The Determination of Optimal W/B Ratio

In compliance with the wet particle-packing method, a series of experiments were conducted to optimize the binder and w/b ratio. Sets of UHPC with MK and UHPC with MS were performed, keeping in mind that UHPC must fall into the criteria as mentioned in the ASTM C1856/C1856M-17 [29]. Figure 5. depicts the results of UHPC with MK and UHPC with MS. Figure 5a. shows that the optimum wet particle-packing density is achieved with an optimum w/b ratio of 0.237, which is approximately 0.24 against a 265 mm slump of UHPC with MK. Whereas, Figure 5b. explains the trend of the compressive strength (MPa) and slump (mm) of UHPC with MK against w/b ratios. At w/b of 0.24, compressive strength of 136.3 MPa was achieved, although it is worth to mentioning that the highest compressive strength of UHPC with MK of 138.5 MPa was measured. Vice versa, very identical results were found for UHPC–MS (Figure 5c,d). An optimum w/c of 0.236 was found, as was 128.5 MPa compression strength, which is approximately 0.24. Hence, for this research work, an optimal w/b ratio was found to be 0.24.

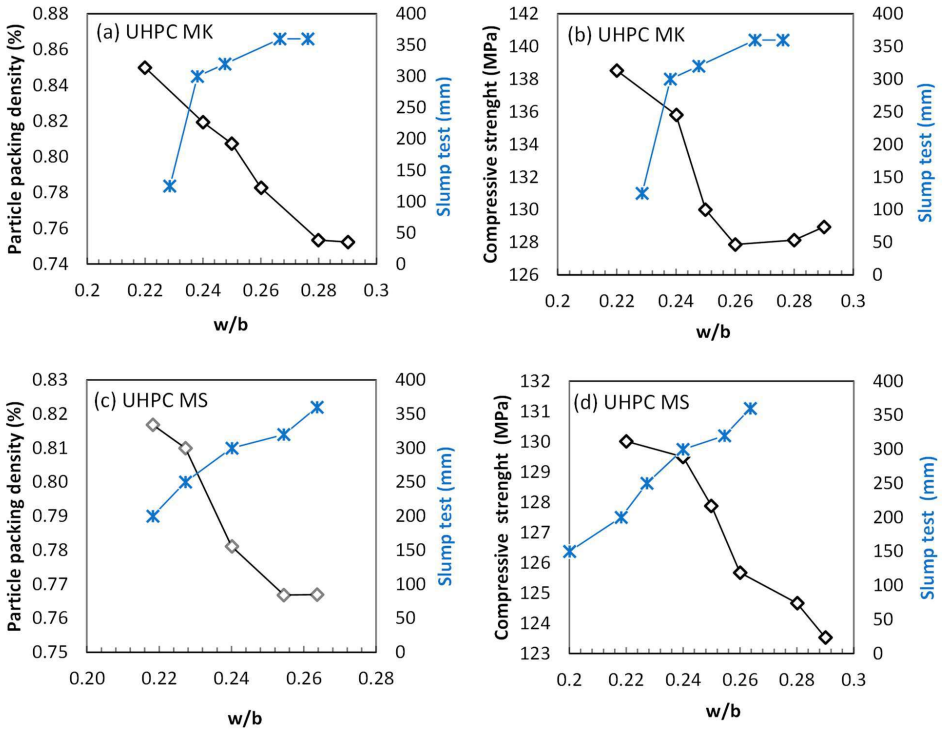

Figure 5. Wet particle-packing density, slump test and compression tests corresponding at diferent w/bs for (**a**,**b**) UHPC–MK. And (**c**,**d**) UHPC–MS.

3.2. Density and Reological Properties

The density of all concrete mixtures is presented in Figure 6a. Both UHPC MK and UHPC MS, owing to their smaller average particle sizes compared to the average cement particle size, fill the voids between the cement grains, thereby increasing the density of the concrete matrix. The additions of MK and MS are observed to raise the density from approximately 2320 kg/m^3 to 2550 kg/m^3 compared to the reference mix. Notably, the density of UHPC MS is slightly lower than that of UHPC MK. This slight decrease may be attributed to a higher porosity in the MS concrete mixtures due to lower particle-packing density, because the specified densities of MK and MS particles are almost equal. Furthermore, Figure 6a shows that the density of UHPC concrete mixtures changes slightly with increasing fiber content. It is to be expected that an increase in the fiber content will increase the density of UHPC mixtures, as the fiber material is heavier than the matrix material. However, a slight decrease in the density of UHPC MS can be observed with increasing fiber content. This can be explained by the increased porosity and air voids, which are mainly due to the fiber distribution in the concrete matrix. For UHPC with MK, the trend is exactly the opposite. This could be due to the better packing of MK compared to MS particles, as can be seen in Figure 5.

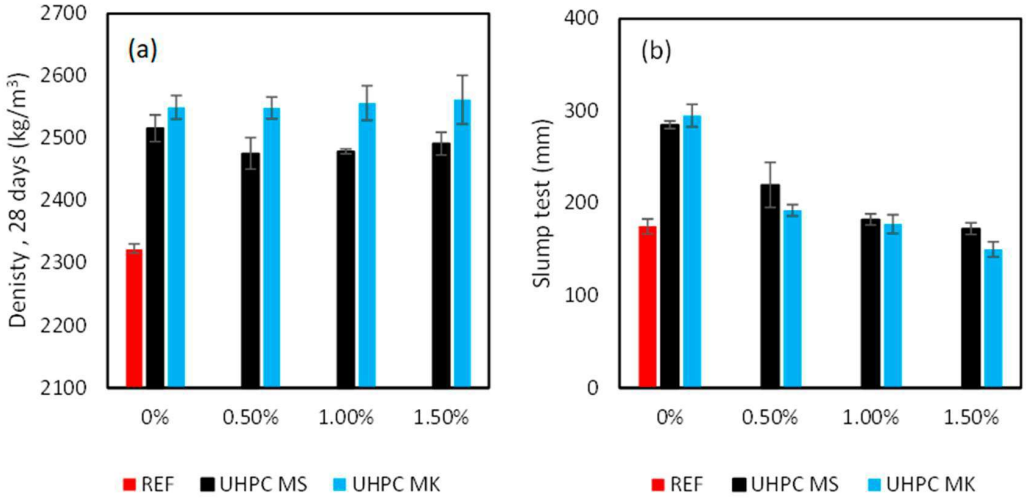

Figure 6. (**a**) Density and (**b**) rheological properties of concrete mixes.

The results of the slump tests of all concrete mixtures together with the standard deviations are shown in Figure 6b. The slump values of UHPC MK and UHPC MS admixtures without fibers are significantly higher than REF concrete. It can be concluded that the optimum addition of MS and MK (10%) improves the particle-packing density of UHPC, due to their small particle sizes compared to the reference mix, and thus increases workability. For example, the slump value of UHPC MK without fibers increased by 69% compared to REF concrete. In contrast, the workability of UHPC mixtures decreased with the addition of basalt fibers. It is obvious that slump values tend to decrease with increasing fiber content. The same tendency was also observed in [41]. The reason for this is that the increasing addition of the fibers restricts the flowability of the mixture due to the increased interactions between the fibers. In this study, the effects of MK and MS on the slump test values of the tested concretes were also compared. With the increase in fiber replacement, the workability of the MK concrete mixtures decreased similarly to that of the MS concrete mixes at all fiber volume fractions. Therefore, the mixtures with 1.5% fibers have the lowest slump value, which corresponds approximately to that of REF concrete. As the fibers have a larger surface area, they require additional water to cover them, which reduces workability.

3.3. Mechanical Properties

Knowledge of the mechanical properties of fiber-reinforced concrete composites is of great importance if they are to be used effectively and economically in practice. The

mechanical properties are influenced by the physical and rheological properties of the concrete mixture such as porosity and degree of workability. According to [8], reduction in porosity and an increase in density leads to an increase in flexural and compressive strength. The compressive strength of hardened composite concrete is a property that depends largely on the composition of the matrix, while the fibers have relatively little influence. This is in contrast to the flexural properties, which are much more dependent on the presence of the fibers and the interactions between the fibers and the matrix.

3.3.1. Compressive and Flexural Strength

Figure 7a shows the mean 28-day compressive strength, along with standard deviations for the REF concrete mixture and the UHPC–MS and MK mixtures with different fiber contents (0%, 0.5%, 1%, and 1.5%). As expected, the compressive strength of the REF concrete mixture is the lowest. Conversely, an increase in compressive strength is observed for all UHPC mixtures. The average compressive strength of all UHPC concrete mixtures ranges from 121 MPa to 136 MPa, classifying all mixtures as UHPC. Moreover, MK and MS increased the concrete strength to almost the same value with the same fiber volume replacement. The UHPC MS concrete mixture without fibers achieved the highest compressive strength, which is 179% higher than that of the REF mixture. The reason for this is the high packing density of the particles (see Figure 5), which leads to smaller voids in the concrete matrix, and thus reduces porosity and improves the compressive strength of the UHPC. In general, all additional cementitious materials improve the strength of the concrete due to very fine particles, enhancing the microstructure by making it denser, more homogeneous, and more uniform than ordinary cement. However, the presence of fibers in UHPC samples slightly reduces the compressive strength compared to UHPC mixtures without fibers. Consequently, the UHPC concrete mixture with the highest fiber volume content obtained the lowest compressive strength. It can be concluded that the addition of basalt fibers has a small negative impact on the compressive capacity of UHPC concrete, with minimal differences between mixtures containing MS and MK. Furthermore, Figures 6b and 7a illustrate that the workability and strength of UHPC concrete are proportional; the compressive strength decreases with decreasing workability. This decrease in compressive strength due to the increase in fiber volume can be explained by the rise in the amount of air voids in the mixture, resulting from poorer workability and insufficient compaction due to fiber agglomeration [7].

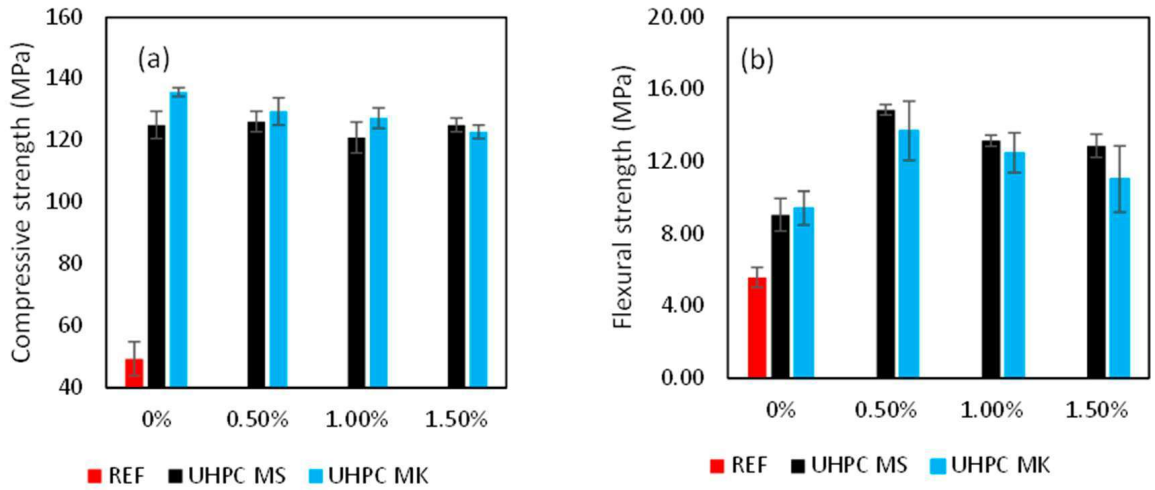

Figure 7. (**a**) Compressive and (**b**) flexural strength of REF, UHPC MU, and UHPC MK at different vol.% of basalt fibers.

Figure 7b shows the mean values of the flexural strength of the tested concrete mixtures together with the standard deviations. As expected, the flexural strength of the REF concrete mix is the lowest. The positive effects of MK and MS on flexural strength can be observed.

Again, the results show almost the same improvement for the addition of MS and MK, about 62% for UHPC MS and about 69% for UHPC MK higher flexural strength than REF concrete. An increase in flexural strength is observed for all UHPC mixes with fibers compared to mixes without fibers. The improvement in strength for UHPC MS concrete mixes is slightly higher than for UHPC MK concrete mixes with fibers. The reason for this could be the better bond strength of the fibers and concrete matrix in MS, as well as better fiber distribution and orientation. The maximum flexural strength is achieved for UHPC concrete mixes with a low fiber volume content of 0.5%. The flexural strength increased by 167% (with MS additive) and 146% (with MK additive) compared to the REF mix, and by 64% (with MS additive) and 46% (with MK additive) compared to UHPC mixes without fibers. On the other hand, a slight downward trend can be observed in UHPC concrete mixes with a fiber volume content of more than 0.5%. A high fiber content can cause the fibers to become entangled with each other, resulting in poor fiber distribution, increased porosity and reduced flexural strength [42].

3.3.2. The Influence of Basalt Fibers on Displacement Fracture

To characterize the flexural behavior of fiber-reinforced concrete composites, it is essential to analyze the load vs. deflection curve, which reflects the impact of fibers in the post-peak zone, including toughness and crack opening. The dosage, distribution, and orientation of fibers are well-known factors influencing the flexural behavior of fiber-reinforced concrete. From the curves presented in Figure 8, substantial differences in the post-peak behavior are evident between mixtures without fibers and those with fibers. Overall, it can be summarized that, following the attainment of the maximum load, the load decreases for all mixes. Additionally, if the volume fraction of basalt fibers in UHPC mixtures is increased, a smaller reduction in load is observed.

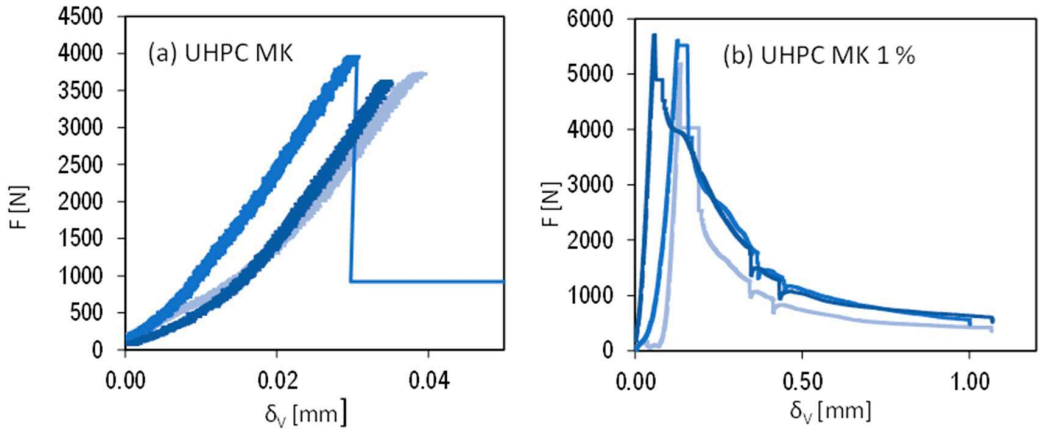

Figure 8. Force vs. displacement for (**a**) UHPC MK without fibers and (**b**) UHPC MK 1% with fibers.

As expected, UHPC with MS and MK and those without fibers fractured in a disastrously brittle way due to their high strengths. Additionally, the laboratory test results indicate that at low fiber concentrations (<0.5%), there was no significant improvement in the post-peak zone. The impact of fibers on brittleness is evident in the load vs. displacement curve, revealing a substantial reduction after incorporating 1% fibers into the UHPC mixture with MK. Comparable or even superior enhancements in post-peak response were noted with the addition of MS. Nevertheless, the increased fiber content has adversely affected both rheological and mechanical properties. Reinforcement with 1 vol% was selected as optimal.

3.4. Microstructure Analysis

In the initial phase, the surface morphology and roughness of the samples was examined, followed by an analysis of the inner microstructure.

3.4.1. Surface Morphology and Roughness

The FE-SEM surface morphology of the REF and UHPC biomimetic are presented in Figure 9. The surface of REF samples is smooth. At a magnification of 10,000, crystals in the form of flake and block structures are visible. The relatively flat surface does not permit the entrapment of air under the formatted droplet, as seen in Figure 9a–c, suggesting that this surface is hydrophilic. Super water-repellent surfaces were successfully fabricated using a combination of surface-covering meshes and a SiO_2 nanoparticle-based spray coating. To synthesize superhydrophobic hierarchical surfaces, it is essential to determine the optimal distance between convex structures made by surface-covering meshes [43]. Figure 9d displays the uneven structure left on the surface of UHPC MK, featuring sub-millimeter convex structures in the shape of squares with the optimal size side sizes of 200 µm, created by the imprinted polyester meshes.

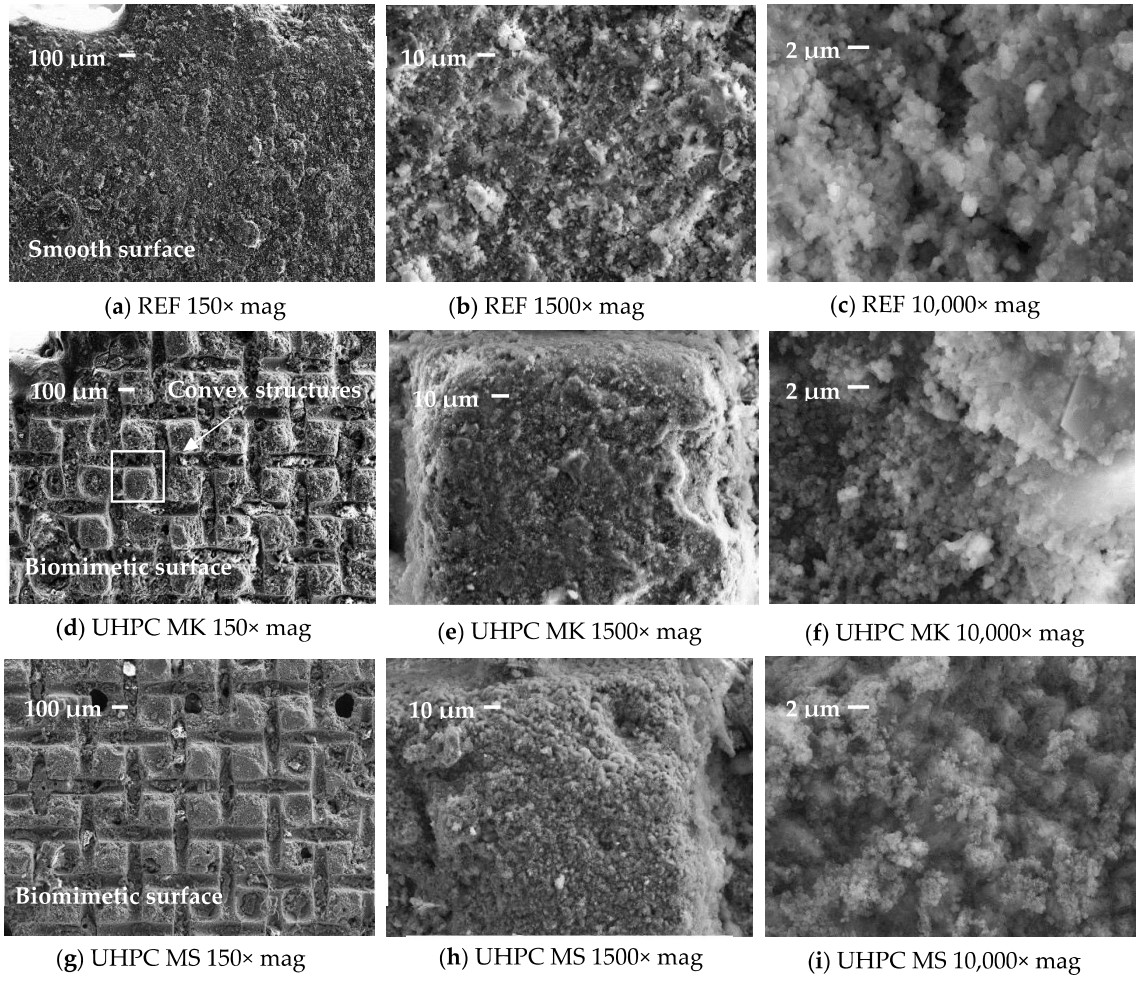

(**a**) REF 150× mag (**b**) REF 1500× mag (**c**) REF 10,000× mag

(**d**) UHPC MK 150× mag (**e**) UHPC MK 1500× mag (**f**) UHPC MK 10,000× mag

(**g**) UHPC MS 150× mag (**h**) UHPC MS 1500× mag (**i**) UHPC MS 10,000× mag

Figure 9. Micrographs of (**a–c**) REF smooth surfaces, (**d–i**) biomimetic UHPC surface at different magnification.

Similar to the lotus leaf, which has micro-papillae and nanofibers, the fabricated biomimetic surface exhibits a multi-scale roughness convex structure with chemically bonded SiO_2 nanoparticles. Numerous nano-size clusters are present, constituting condensed aggregates of SiO_2 nanoparticles. Consequently, the rough superhydrophobic concrete surface exhibits a combination of micro- and nano-scaled structures. The biomimetic surface with both micro- and nano-composite structures was made on both UHPC MK and UHPC MS samples (Figure 9d–i). There are more micro- to nano-scale voids on the surface of biomimetic samples, which can intercept air and greatly reduce the contact area between the surface and the water droplets. A large amount of air is entrapped in the of micro-

and nano-scaled structures under the combined action of imprinted convex structures and cross-linked SiO_2 nanoparticles [33]. This behavior aligns with the structure described by the Cassie–Baxter model that exhibits superhydrophobicity, a self-cleaning effect, and prevents water penetration into the matrix of the samples [44].

The given surface was further enhanced by applying luminescent powder before adding the SiO_2 nanoparticle coating. The textured upper surface, formed by imprinted convex structures and layer by layer spraying, comprised numerous clusters of luminescent powder and SiO_2 nanoparticles. A modified surface with a dual-layered design is presented in Figure 10a,b, where the introduction of a colorless luminescent coating results in a visibly rougher upper surface on the biomimetic cubes. Self-luminescence could also be provided by the internal mixing of the powder in the production of UHPC. However, the use of luminescent powder might lead to the deterioration of mechanical properties, a reduction in workability, and an increase in porosity and overall cost due to the higher quantity required. Therefore, it is recommended to use luminescence powder coatings for UHPC.

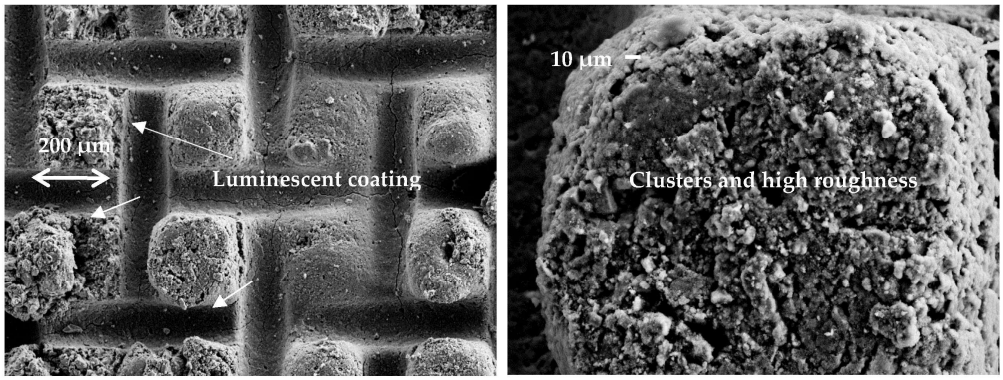

(**a**) UHPC MS-lum 300× mag (**b**) UHPC MS-lum 1500× mag

Figure 10. A modified surface with a dual-layered design; luminescent coating results in a visibly rougher upper surface on the biomimetic cubes at (**a**) 300× magnification and (**b**) 1500× magnification.

Table 3 shows FE-SEM-EDS spectrum of elements present on non-coated REF and UHPC coating only with SiO_2 nanoparticles and UHPC-containing surfaces' dual-layered design with SiO_2 nanoparticles and luminescent coating. The amounts of the elements Ca, Si, and Al in hydrated cement paste primarily influence the structure and performance of key compounds such as C–S–H, $Ca(OH)_2$, $C_3AS_3H_{32}$ (AFt), and C_4ASH_{18} (AFm), ultimately impacting the overall performance of cement-based materials and surfaces [45]. C–S–H, being the principal binding phase in concrete, is the primary hydration product that governs strength, typically characterized by the Ca/Si ratio. Blended cement composites with lower Ca/Si ratios can contribute to improved durability, reduced permeability, and enhanced resistance to chemical attack [46]. The results indicate that the fabricated biomimetic UHPC-containing pozzolans have lower Ca/Si ratios, resulting in more resistant and durable surfaces compared to the REF samples. Furthermore, the surfaces of UHPC MK and UHPC MS are characterized by a predominance of Ca, Si, and O, resulting from the application of a sprayed coating with SiO_2 nanoparticles. In the case of UHPC MK-lum and UHPC MS-lum, which have dual-layered surface designs, the increase in Al and Sr is attributed to the presence of strontium aluminate luminescent powder on the surfaces.

Table 3. FE-SEM-EDS presents spectrum mean averages of the content of elements (wt.%) on non-coated and coated surfaces.

Spectrum	O	Na	Mg	Al	Si	S	Cl	K	Ca	Ti	Mn	Fe	Sr
REF	55.95	0.23	0.28	0.91	7.93	0.07	0.1	2.76	31.23	0.05	0.00	0.23	0.26
UHPC MK	57.24	0.32	0.23	3.95	9.78	0.14	0.03	1.5	24.05	0.12	0.06	0.29	2.27
UHPC MS	58.97	0.42	0.06	0.37	17.37	0.07	0.03	1.08	20.42	0.01	0.00	0.23	0.97
UHPC MK-lum	52.83	0.22	0.09	2.78	35.69	0.23	0.13	0.58	3.35	0.00	0.00	0.02	4.09
UHPC MS-lum	58.92	0.53	0.30	11.19	3.41	1.82	0.32	0.79	1.26	0.03	0.00	0.03	21.46

Based on profilometry measurements, 3D topographic profiles of REF and UHPC MK-lum surfaces are presented in Figure 11. For REF samples, which present lacking fineness in concrete and a high water to cement ratio, the uneven surface is partly filled with hydrated paste, leaving local depressions and protrusions on the surface. Irregular and low roughness on the surface are the main reasons for its hydrophilicity and susceptibility to contamination with dust particles [47]. In the case of the UHPC MK-lum, surfaces with dual-layered designs with micro and nano convex structures are uniformly dispersed on the surface, resulting in a rough surface that is consistent with the Cassie–Baxter model. Voids are visible, representing space for entrapped air, which repels water droplets.

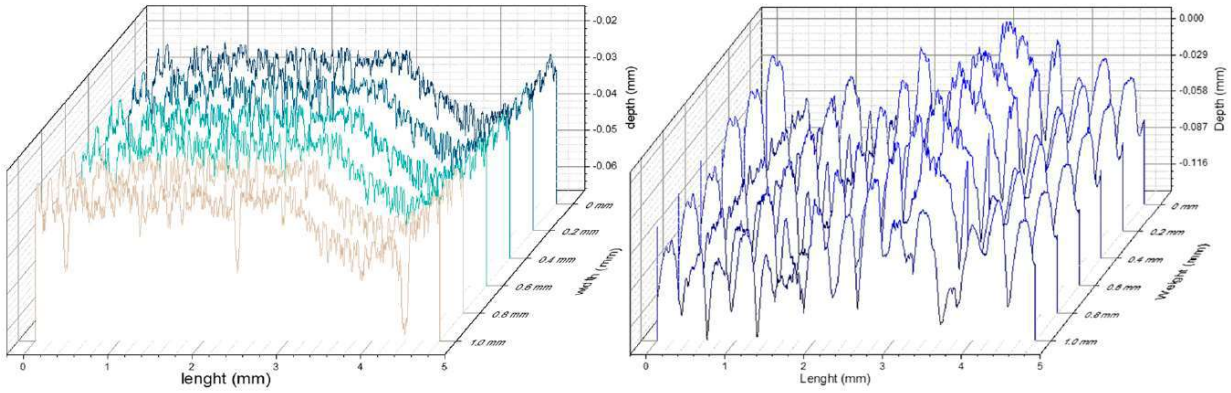

(**a**) REF roughness (**b**) UHPC MK-lum roughness

Figure 11. 3D topographic profiles of (**a**) REF and (**b**) UHPC MK-lum surfaces.

The surface roughness calculation results are presented in Table 4. The parameters are the root mean square roughness (R_q), arithmetic average roughness (R_a), and maximum roughness (R_{MAX}). All parameters are higher in the UHPC MK-lum surfaces compared to the REF surface. For instance, R_{MAX} increases from 26.79 µm on the REF surface to 57.60 µm on the UHPC MK-lum surfaces. The topographic profiles and calculated parameters for both surfaces align with the SEM results.

Table 4. The surface roughness parameters for REF and UHPC MK-lum.

Surface	R_q (µm)	R_a (µm)	R_{MAX} (µm)
REF	2.50	3.59	26.79
UHPC MK-lum	10.16	12.24	57.60

3.4.2. Inner Cross-Section Microstructure and Basalt Fibers

The morphology of the cross-section and distribution of basalt fibers in the hydrated UHPC matrix were observed using SEM-EDX, as given in Figure 12. It can be seen that the surface of basalt fibers is smooth, homogeneously distributed, and well adhered to the UHPC matrix (Figure 12b). Basalt fibers made from the natural product, namely the

volcanic stones, are promised to be a sustainable replacement for the glass and steel fibers in concrete [48]. As expected, the main chemical elements of the basalt fibers are Si, Al, Fe, Ca, and O, which primarily form SiO_2, Al_2O_3, CaO, and FeO (Figure 12d). Interfacial bonding between the hydration crystals of the UHPC matrix and basalt fibers provides sufficient resistance to enhance the post-peak response of the strain curve. The flexural crack passes through the fibers in the matrix, inducing stress into the basalt fibers and forming a physical bridge that absorbs energy after reaching the ultimate load. Similar to the work by Yan et al. [49] during the failure process, the reinforced samples exhibit multiple cracks instead of just one. This is attributed to the effect of fibers, which contribute ductility and are tightly bonded to the matrix. In addition, fibers did not chemically affect the microstructure of the fabricated UHPC composites, and can be used even in severe environments containing chloride and sulphate solutions [50].

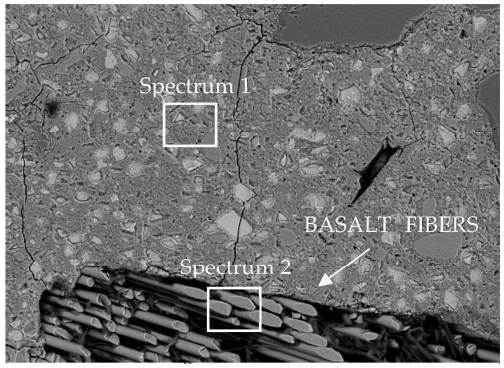

(**a**) UHPC MK 1% 150× mag

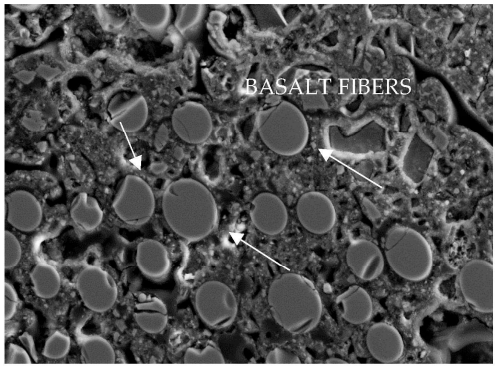

(**b**) UHPC MK 1% 1500× mag

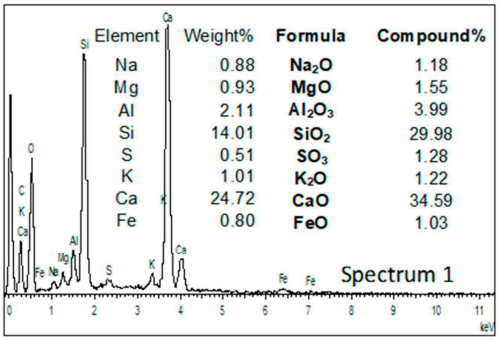

(**c**) Spectrum 1 (cement matrix)

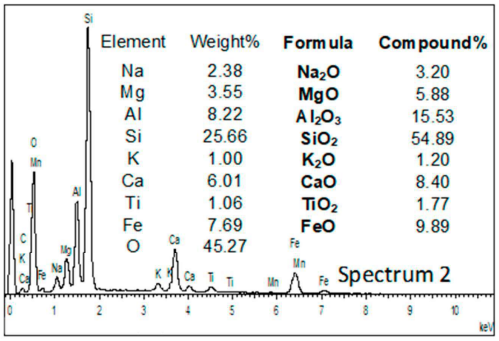

(**d**) Spectrum 2 (basalt fibers)

Figure 12. The inner morphology and distribution of basalt fibers in hydrated UHPC matrix with corresponding FE-SEM-EDS spectra.

3.5. The Contact and Roll of Angles (CA, RA)

Figure 13 shows the CA and RA of the REF, UHPC MK 1%, and UHPC MK 1-lum surfaces. Compared to the droplets on the REF surface (c), those on the coated hydrophilic surfaces (b,c) exhibit a typical spherical shape. Droplets on the REF surface quickly disperse into the concrete matrix, indicating clear hydrophilicity with an average CA of 29.5° and a RA of 95°. On the other hand, UHPC MK 1% already poses superhydrophobicity with an average CA of 151° and RA of 9.2°. When testing the dual-layered design surface containing luminescent powder and SiO_2 nanoparticles, the samples UHPC MK 1-lum and UHPC MS-lum displayed an even greater increase, reaching an average CA of 154.9° and 155.45°, and a RA of 7.5° and 7.1°, respectively. This marks the first report of a superhydrophobic and self-luminescent UHPC surface. Water does not penetrate the biomimetic UHPC surface but floats on air pockets trapped between the uneven surface. Superhydrophobic surfaces have a self-cleaning effect that allows contamination or dust to automatically fall off under the action of gravity, wind, and rain [51]. The droplets could effortlessly roll off the surface, removing dust and at the same time preserving the decorative appearance and

long-lasting self-luminescence performance of UHPC. This innovative low-cost superhydrophobic and self-luminescent UHPC surface has high applicability and can potentially boost sustainability in construction.

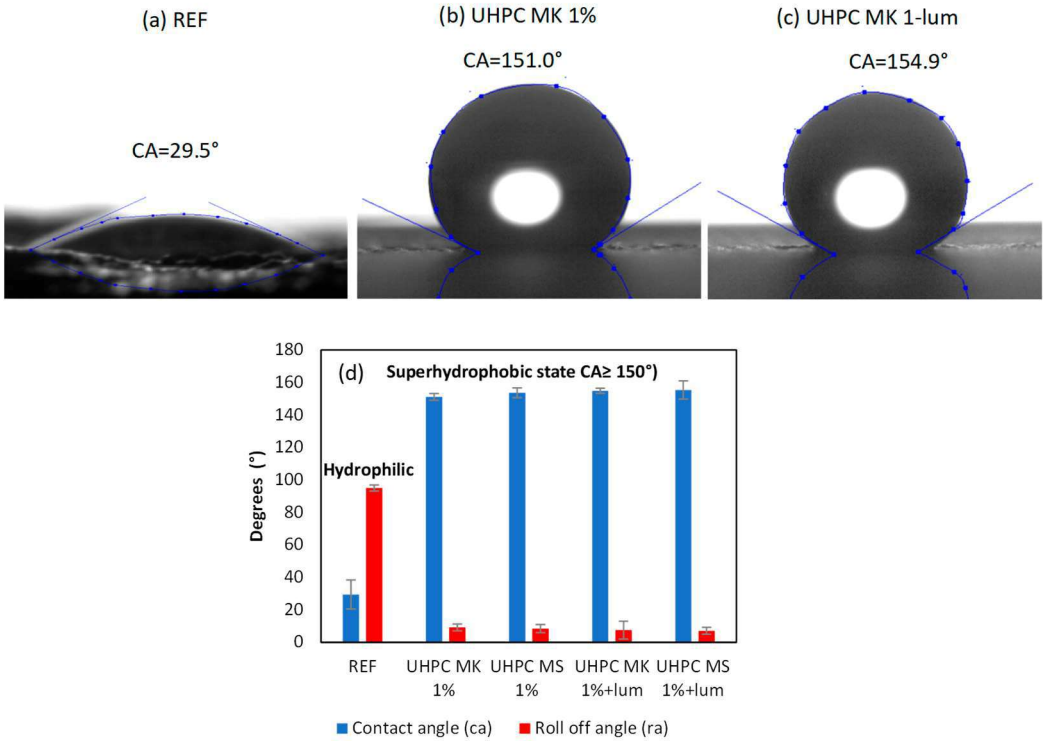

Figure 13. (**a**) Droplets on the hydrophilic surface. (**b**) super repellant one-layered biomimetic SiO_2 coated UHPC surface, and (**c**) dual-layered design UHPC surface. (**d**) When dual-layered coated, samples displayed an even greater increase, having a superhydrophobic state (CA $\geq$ 150°, RO $\leq$ 10°).

3.6. Self-Luminiscence

Figure 14 shows that UHPC MK 1%-lum and UHPC MS 1%-lum can emit yellowish-green light in the dark. It was observed that the initial emitted light intensity is the highest. In the first 30 min, the decay rate of the emitted intensity was the fastest and then slowed down. Self-luminescence was more intense in UHPC MK 1%-lum compared to UHPC MS 1%-lum. The reason for this is the use of the pozzolanic additive; MS, compared to MK, darkens the appearance of UHPC and reduces the intensity of light emission. As measured in Figure 14, the peak wavelength of the emission spectrum was 520 nm, corresponding to the yellowish-green light wavelength visible to the human eye.

Luminescence coating on the sample surface absorbs energy from ultraviolet or solar light, leading to the creation of self-luminescence. This involves the generation and migration of electron holes, which are then captured by certain defect levels in the material. Over time, these captured holes return their energy to the surroundings, and the afterglow is produced through the recombination of electrons with excited electrons in specific energy levels [52]. In simple terms, the substance glows in the dark after being exposed to light, making it useful for applications like visible signage or illuminating surfaces composed of UHPC without relying on external lighting.

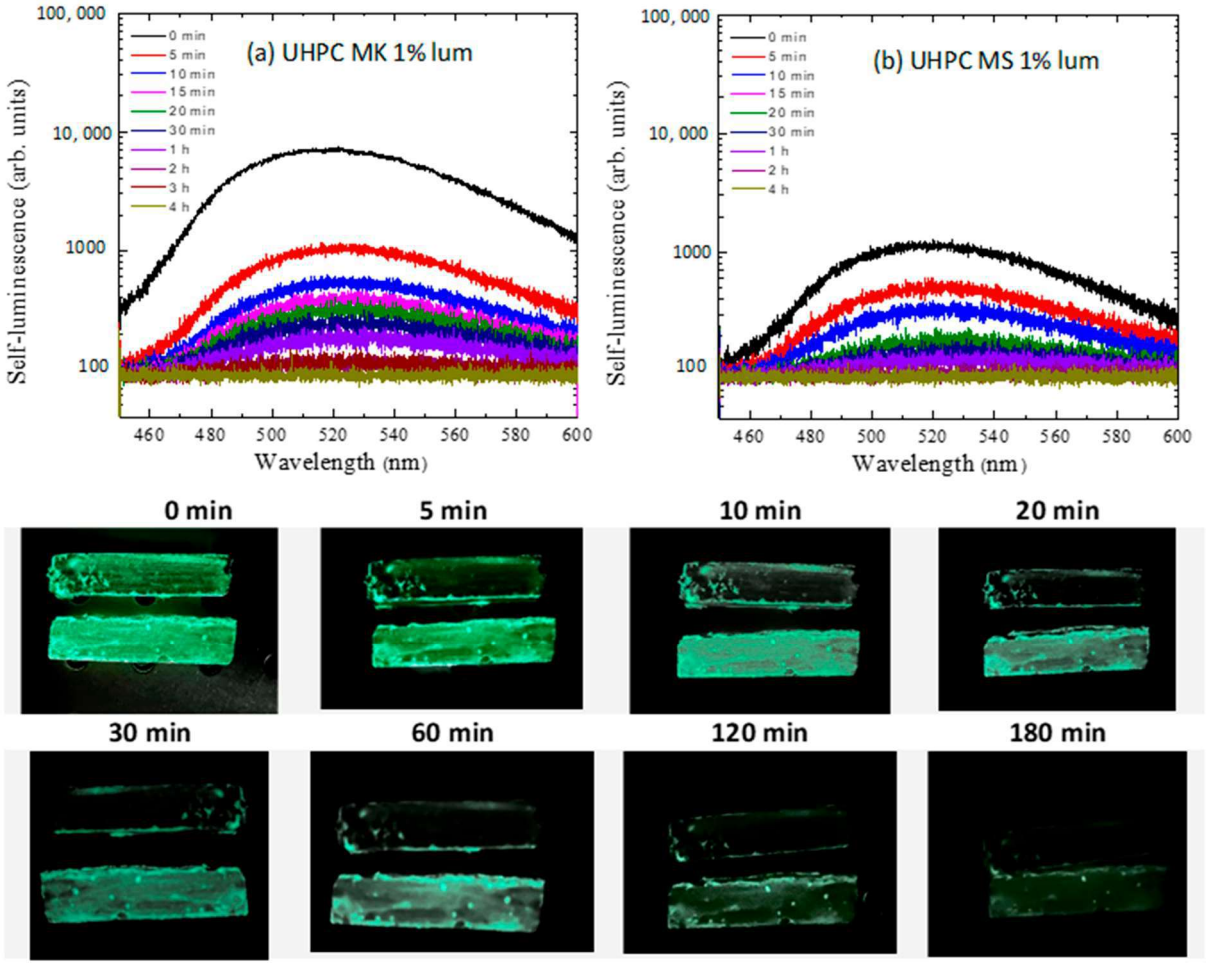

Figure 14. Self-luminesce peak wavelength and intensity vs. time for UHPC MK 1%-lum and UHPC MS 1%-lum.

4. Conclusions and Future Prospectives

Ultra-high-performance concrete (UHPC) stands as a revolutionary material in modern construction, renowned for its exceptional strength and durability. In pursuit of sustainable practices in civil engineering, new green formulations of UHPC were developed, incorporating supplementary cementitious materials and basal fibers as alternative concrete reinforcement. In the first phase, an optimal water-to-binder ratio was determined to align it with high particle-packing density, excellent rheological properties, and high compression strength. When introducing basalt fibers, the 1 vol.% mixture was chosen as the ideal for fabricating multifunctional UHPC with sufficient ductility. The objective was to enhance the functionality and long-lasting visual appearance of decorative UHPC. Simultaneously, the objective was to reduce the energy consumption associated with the nighttime lighting of UHPC infrastructure. A novel cost- and time-effective fabrication strategy for an advanced light-emitting biomimetic surface design of UHPC was introduced.

With the average compressive strength categorizing the blends as UHPC, flexural strength notably increases, compared to the reference mix. Basalt fibers contribute to enhanced post-peak strain responses and notable reductions in brittleness. The surfaces of REF samples have a smooth surface, making them hydrophilic and susceptible to dust. The surface of self-luminance biomimetic samples exhibits more micro to nano-scale voids. Regarding inner microstructure, the surface of basalt fibers is observed to be smooth, homogeneously distributed, and well-adhered to the UHPC matrix. Wettability tests show increased contact angles and reduced roll-off angles in UHPC MK and UHPC MS samples, indicating super water repellency and self-cleaning properties. Self-luminescence features

show an initial peak in emitted light intensity, with more intensity observed in UHPC MK 1%-lum compared to UHPC MS 1%-lum.

The future of UHPC with superhydrophobic and self-luminescent features holds great promise for transforming civil engineering and infrastructure development. Adding superhydrophobic properties to UHPC surfaces can increase durability, lower maintenance costs, and improve resistance to environmental pollutants. At the same time, incorporating self-luminescent properties offers an innovative solution for energy-efficient nighttime lighting. By using luminescent materials within the concrete, UHPC structures can emit light without external energy sources, reducing energy consumption and environmental impact. Ongoing research in these areas could lead to more innovations, better materials, and broader use in real-world projects. As the construction industry increasingly focuses on sustainability and energy efficiency, UHPC with these advanced properties is expected to play a crucial role in shaping future infrastructure from high-rise buildings and bridge decks to wind turbine foundations.

Author Contributions: Conceptualization, G.K.; methodology, G.K., N.B.O., N.G., A.C. and M.P.; validation, A.I. and S.L.; investigation, G.K., N.B.O., N.G., A.C., M.P., A.I. and S.L.; resources, A.C., N.G. and N.B.O.; data curation, A.R.M., G.K., N.B.O., N.G. and M.P.; writing—original draft preparation, A.R.M., G.K. and N.B.O.; writing—review and editing, G.K. and N.B.O.; supervision, G.K. and A.C. All authors have read and agreed to the published version of the manuscript.

Funding: This research received no external funding.

Institutional Review Board Statement: Not applicable.

Informed Consent Statement: Not applicable.

Data Availability Statement: The data presented in this study are available on request from the corresponding author.

Acknowledgments: The authors would like to acknowledge the Erasmus+ program and the Slovenian Research Agency (ARRS) for partially financing this research within the framework of program P2-0046. Mechanical tests were carried out on equipment purchased under the project 'Research Infrastructure for Campus-based Laboratories' at the University of Rijeka, with the number RC.2.2.06-0001, co-funded by the European Fund for Regional Development (ERDF). FE-SEM-EDS and 3D topography analyses were conducted in the Department of Chemistry and Industrial Chemistry, University of Geneva, Italy. Self-luminescence tests were conducted at the Institute of Materials Science, Universidad de Valencia, Valencia, Spain. Special thanks to the esteemed visiting researchers Rene Gomolj and Doris Markač. Many thanks to students Nikolina Škrilec, Živa Doberšek, Dejana Markova, Nikolina Škrilec, Jan Čokolič, Nejc Časar, David Virag, and technician Aljaž Visinski for helping with our experiments.

Conflicts of Interest: The authors declare no conflicts of interest.

References

1. Abdal, S.; Mansour, W.; Agwa, I.; Nasr, M.; Abadel, A.; Onuralp Özkılıç, Y.; Akeed, M.H. Application of Ultra-High-Performance Concrete in Bridge Engineering: Current Status, Limitations, Challenges, and Future Prospects. *Buildings* **2023**, *13*, 185. [CrossRef]
2. Amran, M.; Huang, S.-S.; Onaizi, A.M.; Makul, N.; Abdelgader, H.S.; Ozbakkaloglu, T. Recent trends in ultra-high performance concrete (UHPC): Current status, challenges, and future prospects. *Constr. Build. Mater.* **2022**, *352*, 129029. [CrossRef]
3. Li, J.; Wu, Z.; Shi, C.; Yuan, Q.; Zhang, Z. Durability of ultra-high performance concrete—A review. *Constr. Build. Mater.* **2020**, *255*, 119296. [CrossRef]
4. Gu, Z.; Feng, H.; Gao, D.; Zhao, J.; Wei, C.; Wu, C. Fatigue Behavior and Calculation Methods of High Strength Steel Fiber Reinforced Concrete Beam. *Sustain. Struct.* **2023**, *3*, 28. [CrossRef]
5. Dong, L.; Yang, Y.; Liu, Z.; Yang, T.; Xue, C.; Shao, R.; Wu, C. Effect of chloride ion migration behaviour on the microstructure and mechanical properties of ultra-high performance concrete: A review. *J. Build. Eng.* **2023**, *82*, 108233. [CrossRef]
6. Chen, Z.; Wang, X.; Ding, L.; Jiang, K.; Huang, H.; Liu, J.; Wu, Z. Synergistic effects of hybrid macro basalt fibers and micro fibers on the mechanical properties of UHPC. *Arch. Civ. Mech. Eng.* **2023**, *23*, 264. [CrossRef]
7. Thomoglou, A.K.; Falara, M.G.; Gkountakou, F.I.; Elenas, A.; Chalioris, C.E. Influence of Different Surfactants on Carbon Fiber Dispersion and the Mechanical Performance of Smart Piezoresistive Cementitious Composites. *Fibers* **2022**, *10*, 49. [CrossRef]

8. Thomoglou, A.K.; Fantidis, J.G.; Voutetaki, M.E.; Metaxa, Z.S.; Chalioris, C.E. Mechanical Characterization of Nano-Reinforced Mortar: X-ray Micro-CT for 3D Imaging of Microstructure. *Eng. Proc.* **2023**, *41*, 4.
9. Wang, D.; Shi, C.; Wu, Z.; Xiao, J.; Huang, Z.; Fang, Z. A review on ultra high performance concrete: Part II. Hydration, microstructure and properties. *Constr. Build. Mater.* **2015**, *96*, 368–377. [CrossRef]
10. Amran, M.; Murali, G.; Makul, N.; Tang, W.; Alluqmani, A.E. Sustainable development of eco-friendly ultra-high performance concrete (UHPC): Cost, carbon emission, and structural ductility. *Constr. Build. Mater.* **2023**, *398*, 132477. [CrossRef]
11. Tasiopoulou, T.; Katsourinis, D.; Giannopoulos, D.; Founti, M. Production-Process Simulation and Life-Cycle Assessment of Metakaolin as Supplementary Cementitious Material. *Eng* **2023**, *4*, 761–779. [CrossRef]
12. Luo, Z.; Zhi, T.; Liu, X.; Yin, K.; Pan, H.; Feng, H.; Song, Y.; Su, Y. Effects of different nanomaterials on the early performance of ultra-high performance concrete (UHPC): C–S–H seeds and nano-silica. *Cem. Concr. Compos.* **2023**, *142*, 105211. [CrossRef]
13. Wu, Z.; Shi, C.; Khayat, K.H.; Wan, S. Effects of different nanomaterials on hardening and performance of ultra-high strength concrete (UHSC). *Cem. Concr. Compos.* **2016**, *70*, 24–34. [CrossRef]
14. Tayeh, B.A.; Askar, L.K.; Bakar, B.A. Ultra-High-Performance Concrete (UHPC)-Applications Worldwide: A State-of-the-Art Review. *J. Eng. Res. Technol.* **2023**, *10*, 12–17.
15. Wu, Y.; Shen, Y.; Tao, J.; He, Z.; Xie, Y.; Chen, H.; Jin, M.; Hou, W. Facile spraying fabrication of highly flexible and mechanically robust superhydrophobic F-SiO2@PDMS coatings for self-cleaning and drag-reduction applications. *New J. Chem.* **2018**, *42*, 18208–18216. [CrossRef]
16. Ratan, J.K.; Saini, A. Enhancement of photocatalytic activity of self-cleaning cement. *Mater. Lett.* **2019**, *244*, 178–181. [CrossRef]
17. Shen, C.H.; Hsu, T.J. Research on vehicle trajectory prediction and warning based on mixed neural networks. *Appl. Sci.* **2021**, *11*, 7. [CrossRef]
18. Ge-Zhang, S.; Cai, T.; Yang, H.; Ding, Y.; Song, M. Biology and nature: Bionic superhydrophobic surface and principle. *Front. Bioeng. Biotechnol.* **2022**, *10*, 1033514. [CrossRef] [PubMed]
19. Wang, F.; Xie, T.; Lei, S.; Ou, J.; Li, W.; Xue, M.; Huang, D. Preparation and properties of foundry dust/Portland cement based composites and superhydrophobic coatings. *Constr. Build. Mater.* **2020**, *246*, 118466. [CrossRef]
20. Yin, B.; Xu, H.; Fan, F.; Qi, D.; Hua, X.; Xu, T.; Liu, C.; Hou, D. Superhydrophobic coatings based on bionic mineralization for improving the durability of marine concrete. *Constr. Build. Mater.* **2023**, *362*, 129705. [CrossRef]
21. Binrui, W.; Qiong, Q.; Xuan, J.; Dong, X.; Liping, S.; Xin, C.; Qizhi, Z.; Feiyan, F.; Xian, Y. A highly robust, concrete-inspired superhydrophobic nanocomposite coating. *Nanoscale* **2023**, *15*, 19304–19313. [CrossRef] [PubMed]
22. Kravanja, G.; Godec, R.F.; Rozman, M.; Rudolf, R.; Ivanič, A. Biomimetic superhydrophobic concrete with enhanced anticorrosive, freeze thaw, and deicing resistance. *Adv. Eng. Mater.* **2022**, *24*, 2101445. [CrossRef]
23. Cirisano, F.; Ferrari, M. Superhydrophobicity and durability in recyclable polymers coating. *Sustainability* **2021**, *13*, 8244. [CrossRef]
24. Wang, W.; Sha, A.; Lu, Z.; Jia, M.; Jiang, W.; Liu, Z.; Yuan, D. Self-luminescent cement-based composite materials: Properties and mechanisms. *Constr. Build. Mater.* **2021**, *269*, 121267. [CrossRef]
25. Voravanicha, K.; Leelachao, S.; Sahasithiwat, S.; Kumnorkaew, P.; Dangtungee, R. Natural rubber filled with phosphorescent materials for pavement. *Mater. Today Proc.* **2019**, *17*, 1971–1976. [CrossRef]
26. Zhu, C.; Lv, J.; Chen, L.; Lin, W.; Zhang, J.; Yang, J.; Feng, J. Dark, heat-reflective, anti-ice rain and superhydrophobic cement concrete surfaces. *Constr. Build. Mater.* **2019**, *220*, 21–28. [CrossRef]
27. Ahmad, M.R.; Pan, Y.; Chen, B. Physical and mechanical properties of sustainable vegetal concrete exposed to extreme weather conditions. *Constr. Build. Mater.* **2021**, *287*, 123024. [CrossRef]
28. Hassan, O.A. An integrated approach to assessing the sustainability of buildings. *J. Eng. Des. Technol.* **2016**, *14*, 835–850. [CrossRef]
29. *ASTM C1856/C1856M-17*; Standard Practice for Fabricating and Testing Specimens of Ultra-High Performance Concrete. ASTM International: West Conshohocken, PA, USA, 2017; pp. 1–4.
30. *SIST EN 1015-3*; Determination of Consistance of Sresh Mortar (by Low Table). SIF Standardization: Noordwijk, The Netherlands, 2001.
31. *ASTM C109/C109M-99*; Standard Test Method for Compressive Strength of Hydraulic Cement Mortars (Using 2-in. or [50-mm] Cube Specimens). ASTM International: West Conshohocken, PA, USA, 2017; p. 6. [CrossRef]
32. *HRN EN 196-1*; Methods of Testing Cement—Part 1: Determination of Strength. Zagreb, Croatia, 2016. Available online: https://standards.iteh.ai/catalog/standards/cen/37b8816e-4085-4dcc-a642-a383d9bddd6c/en-196-1-2016 (accessed on 27 December 2023).
33. Yuan, Q.; Shi, C.; He, T. Design and performance optimization of self-cleaning coating on decorative UHPC surface. *Constr. Build. Mater.* **2023**, *394*, 132115. [CrossRef]
34. *SIST EN 12390-1:2021*; Testing Hardened Concrete—Part 1: Shape, Dimensions and Other Requirements for Specimens and Moulds. Slovenski Inštitut za Standardizacijo: Ljubljana, Slovenia, 2021.
35. *SIST EN 12390-2:2019*; Testing Hardened Concrete—Part 2: Making and Curing Specimens for Strength Tests. Slovenski Inštitut za Standardizacijo: Ljubljana, Slovenia, 2019.
36. Chu, S.H.; Lam, W.L.; Li, L.; Poon, C.S. Packing density of ternary cementitious particles based on wet packing method. *Powder Technol.* **2022**, *405*, 117493. [CrossRef]
37. Shi, C.; Wu, Z.; Xiao, J.; Wang, D.; Huang, Z.; Fang, Z. A review on ultra high performance concrete: Part I. Raw materials and mixture design. *Constr. Build. Mater.* **2015**, *101*, 741–751. [CrossRef]

38. Park, S.; Wu, S.; Liu, Z.; Pyo, S. The role of supplementary cementitious materials (SCMs) in ultra high performance concrete (UHPC): A review. *Materials* **2021**, *14*, 1472. [CrossRef]
39. Ocelić, A.; Baričević, A.; Smrkić, M.F. Synergistic Integration of Waste Fibres and Supplementary Cementitious Materials to enhance sustainability of Ultra-High-Performance Concrete (UHPC). *Case Stud. Constr. Mater.* **2023**, *20*, e02772. [CrossRef]
40. Huang, E.; Skoufis, A.; Denning, T.; Qi, J.; Dagastine, R.R.; Tabor, R.F.; Berry, J.D. OpenDrop: Open-source software for pendant drop tensiometry & contact angle measurements. *J. Open Source Softw.* **2021**, *6*, 2604.
41. Li, Y.-F.; Hung, J.-Y.; Syu, J.-Y.; Chang, S.-M.; Kuo, W.-S. Influence of sizing of basalt fiber on the mechanical behavior of basalt fiber reinforced concrete. *J. Mater. Res. Technol.* **2022**, *21*, 295–307. [CrossRef]
42. Al-Ameen, E.; Blanco, A.; Cavalaro, S. Durability, permeability, and mechanical performance of sprayed UHPC, as an attribute of fibre content and geometric stability. *Constr. Build. Mater.* **2023**, *407*, 133393. [CrossRef]
43. Song, J.; Li, Y.; Xu, W.; Liu, H.; Lu, Y. Inexpensive and non-fluorinated superhydrophobic concrete coating for anti-icing and anti-corrosion. *J. Colloid Interface Sci.* **2019**, *541*, 86–92. [CrossRef] [PubMed]
44. Chang, Z.; Lu, Y. Fabrication of superhydrophobic surfaces with Cassie-Baxter state. *J. Dispers. Sci. Technol.* **2022**, *43*, 1099–1111. [CrossRef]
45. Wu, Z.; Khayat, K.H.; Shi, C.; Tutikian, B.F.; Chen, Q. Mechanisms underlying the strength enhancement of UHPC modified with nano-SiO_2 and nano-$CaCO_3$. *Cem. Concr. Compos.* **2021**, *119*, 103992. [CrossRef]
46. Erdem, S.; Dawson, A.R.; Thom, N.H. Influence of the micro-and nanoscale local mechanical properties of the interfacial transition zone on impact behavior of concrete made with different aggregates. *Cem. Concr. Res.* **2012**, *42*, 447–458. [CrossRef]
47. Lapidus, A.; Korolev, E.; Topchiy, D.; Kuzmina, T.; Shekhovtsova, S.; Shestakov, N. Self-cleaning cement-based building materials. *Buildings* **2022**, *12*, 606. [CrossRef]
48. Overkamp, T.; Mahltig, B.; Kyosev, Y. Strength of basalt fibers influenced by thermal and chemical treatments. *J. Ind. Text.* **2018**, *47*, 815–833. [CrossRef]
49. Yan, P.; Chen, B.; Afgan, S.; Haque, M.A.; Wu, M.; Han, J. Experimental research on ductility enhancement of ultra-high performance concrete incorporation with basalt fibre, polypropylene fibre and glass fibre. *Constr. Build. Mater.* **2021**, *279*, 122489. [CrossRef]
50. Afroz, M.; Patnaikuni, I.; Venkatesan, S. Chemical durability and performance of modified basalt fiber in concrete medium. *Constr. Build. Mater.* **2017**, *154*, 191–203. [CrossRef]
51. Luo, J.; Xu, Y.; Chu, H.; Yang, L.; Song, Z.; Jin, W.; Wang, X.; Xue, Y. Research on the Performance of Superhydrophobic Cement-Based Materials Based on Composite Hydrophobic Agents. *Materials* **2023**, *16*, 6592. [CrossRef]
52. He, B.; Gao, Y.; Qu, L.; Duan, K.; Zhou, W.; Pei, G. Characteristics analysis of self-luminescent cement-based composite materials with self-cleaning effect. *J. Clean. Prod.* **2019**, *225*, 1169–1183. [CrossRef]